Geophys. Astrophys. Fluid Dynamics, Vol. 92, pp. 1–29
Reprints available directly from the publisher
Photocopying permitted by license only

SUCCESSIVE FORMATION OF PLANETARY LENSES IN AN INTERMEDIATE LAYER

HIDENORI AIKI* and TOSHIO YAMAGATA

Department of Earth and Planetary Physics, Graduate School of Science, The University of Tokyo, 7-3-1, Hongo, Bunkyo-ku, Tokyo 113-0033, Japan

(Received 31 August 1999; In final form 6 January 2000)

We study the formation of lenses of the ocean's intermediate water using a 2.5-layer β-plane primitive equation model with localized injection of water mass. For the injecting rate of 1.0 Sv, we have observed that strong vortices are shed regularly. These vortices propagate westward much faster than the second baroclinic long Rossby wave. They are totally isolated from each other and show strong baroclinicity as well. Moreover, they remain stable over a sufficiently long period of time. Regular formation of such strong vortices in the intermediate layer has not been reported previously. The translation speed is explained using the Euler's momentum integral theorem for the nonlinear baroclinic vortex on the β-plane. We have demonstrated that coupling between the primary motion in the intermediate layer and the secondary motion in the upper layer with a meridional shift is crucial to the fast westward translation of the intense vortices. A simple dispersion formula relating the zonal translation speed with the vortex radius is also derived under the assumption of quasi-geostrophy. It has turned out that the analytical relation explains the numerical results surprisingly well despite the limitation of its derivation.

Keywords: Lens formation; intense coherent vortex; North Pacific Intermediate Water; planetary geostrophic dynamics

1. INTRODUCTION

The North Pacific Intermediate Water (NPIW) is a less saline water mass subducted from the surface layer mostly by winter cooling in the

*Corresponding author. Tel.: +81-3-5841-4296, Fax: +81-3-5841-8791, e-mail: ~~aiki@eps.geoph.s.u-tokyo.ac.jp~~
aiki@jamstec.go.jp

subarctic western North Pacific (Talley *et al.*, 1995; Yasuda *et al.*, 1996). Since the NPIW is relatively rich in fresh water, it only reaches an intermediate depth of about 1000 m and spreads out over a wide area in the North Pacific as a major player of the active intermediate depth circulation. Actually, the NPIW originates in the northwestern part of the North Pacific and spreads along the 26.8 σ_θ density surface with a salinity minimum as far as 10°N (Talley, 1988, 1991). Since the water mass survives for around several decades, it may cause decadal/interdecadal climate variation after a long journey to the tropics by releasing its long memory of ocean-atmosphere mixing processes. Watanabe *et al.* (1994), based on the analysis of CFC (chlorofluorocarbon) distributions, estimated the time for the NPIW to travel from the subarctic zone to 10°N at around 30 years. The formation rate was suggested to be approximately 24 Sv (Watanabe *et al.*, 1997). In addition, the NPIW has drawn attention recently as one of missing sinks of carbon dioxide (Tsunogai *et al.*, 1993).

Interestingly, submesoscale strong lenses are often observed in the area where the intermediate water is formed. Maximenko and Yamagata (1995), using moored buoy data of the Megapolygon-87 experiment, reported existence of a lens-shape anticyclonic vortex with a diameter of 40 km at 1200 m depth in the Kuroshio-Oyashio confluent zone at 39°N, 156°E. The rotation rate near the core of the vortex was found to be about $0.5f$, where f denotes the Coriolis parameter. The vortex is classified into submesoscale, coherent vortices (SCVs) in general (McWilliams, 1985). Maximenko *et al.* (1997) have recently reported the evidence suggesting that those lenses are formed by frontal convection of cold, less saline water in the subarctic western North Pacific.

Such lenses, saline or less saline, with intense rotation in the intermediate layer are ubiquitous in the world oceans. For example, the Meddies in the Atlantic, which originate in the Mediterranean Sea are well-known (Armi and Zenk, 1984). Richardson *et al.* (1989) tracked Meddies for two years; those lenses were approximately 100 km in diameter, 800 m in thickness, and $0.2f$ in rotation rate. The Reddies (Red Sea Eddies) and Peddies (Persian Gulf Eddies) are also reported (*cf.* Shapiro and Meschanov, 1991). The ubiquity suggests existence of robust nonlinear dynamics regarding the formation of those isolated intense mesoscale vortices at the intermediate depth.

In this study, the dynamics related to the formation of those intermediate water lenses will be discussed in detail using an idealized model with a constant localized source of the intermediate water mass from the viewpoint of geophysical fluid dynamics. In this sense, the present work is along the line of Davey and Killworth (1989) and Yamagata *et al.* (1990). However, the former authors adopted the 1.5-layer model and missed the important dynamics arising from interaction among different layers. The latter authors addressed their attention more or less to formation of coherent vortices within limited dynamical regimes. Our results are also relevant to laboratory experiments on coherent vortices produced by a source or sink of fluid mass on a sloping bottom. In particular, Whitehead *et al.* (1990) discussed two-layer baroclinic vortices and examined theoretical constraints based on the Euler's momentum integral theorem. Zatsepin and Didkovskii (1996) demonstrated periodic formation of barotropic vortices and suggested a simple shedding mechanism determined by the forcing rate and drift velocity. Cenedese and Linden (1999) adopted a continuous source or sink of mass in a two-layer rotating fluid with a sloping bottom. They have found that the vortex shedding occurs at higher flow rates. The overall limitation of laboratory experiments, however, is the difficulty of realizing the planetary β-effect in a layered model. Therefore we adopt a numerical method to study the vortex formation in the present study.

In Section 2, we formulate the problem as simply as possible using a 2.5-layer primitive equation model. Numerical results with a localized buoyancy forcing are shown in Section 3, in which three distinct dynamical regimes are described. In particular, a successive formation of anticyclonic lenses propagating westward is shown for the first time in a strongly nonlinear regime. In Section 4, we suggest usefulness of the concept of the beta spiral to explain the simulation results. The fast migration speed of the strongly nonlinear vortex is explained using a steady nonlinear solution for the quasi-geostrophic potential vorticity equation. Section 5 is devoted to summary and discussion.

2. FORMULATION

In order to capture basic features of anticyclonic lens formation at the intermediate depth level, we adopt a 2.5-layer primitive equation

model with active upper and intermediate layers (Fig. 1). The intermediate layer is kept thin in order to mimic the lens structure as much as possible. A β-plane is used to simulate variation of the effective rotation rate with latitude. This will turn out to be the simplest model allowing formation of lenses in the intermediate layer. Since our main purpose is to examine how the intermediate lenses form after surface water is introduced into the intermediate layer, we need to mimic the subduction process in a simple way. Therefore we assume a localized source of water mass in the intermediate layer. This has enabled us to skip the subduction process and to focus our attention on the subsequent evolution of the subducted water mass. The layer model introduces density jumps between neighboring layers, yielding reduced gravity accelerations: $g_{um}=g(\rho_m-\rho_u)/\rho_m$ and $g_{ml}=g(\rho_l-\rho_m)/\rho_m$, where subscripts (u,m,l) denote upper, intermediate(middle) and lower layer, respectively. Adopting the injection of mass Q in the continuity equation of the intermediate layer,

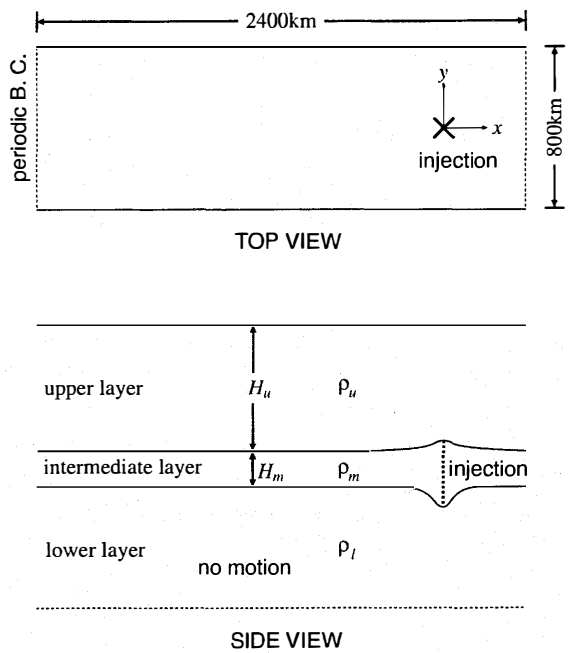

FIGURE 1 Schematic picture of the 2.5-layer model with a localized source of mass.

we can write governing equations as

$$\frac{D\hat{\mathbf{u}}^u}{Dt} + (f_0 + \beta y)\hat{\mathbf{z}} \times \hat{\mathbf{u}}^u = -g_{um}\nabla h^u - g_{ml}\nabla(h^u + h^m), \tag{2.1}$$

$$\frac{\partial h^u}{\partial t} + \nabla\cdot(\hat{\mathbf{u}}^u h^u) = 0, \tag{2.2}$$

$$\frac{D\hat{\mathbf{u}}^m}{Dt} + (f_0 + \beta y)\hat{\mathbf{z}} \times \hat{\mathbf{u}}^m = -g_{ml}\nabla(h^u + h^m) - \frac{Q}{h^m}\hat{\mathbf{u}}^m, \tag{2.3}$$

$$\frac{\partial h^m}{\partial t} + \nabla\cdot(\hat{\mathbf{u}}^m h^m) = Q, \tag{2.4}$$

where $\hat{\mathbf{u}}^i = (u^i, v^i)$, $(i = u, m)$ are horizontal components of velocity in each layer and h^i are layer thicknesses. The other notations are conventional: the Coriolis parameter $f = f_0 + \beta y$ on a β-plane, the Lagrangian derivative $D/Dt = \partial/\partial t + \hat{\mathbf{u}}^i \cdot \nabla$ together with the horizontal gradient operator $\nabla = (\partial/\partial x, \partial/\partial y)$.

The last term in (2.3) is necessary to be consistent in the momentum balance throughout injection; it is neglected in Davey and Killworth (1989) in their 1.5-layer model. It has turned out, however, that the result is not sensitive to the existence of this correction term. We assume a localized source of mass as follows by use of a Gaussian form with amplitude A and radius R_I:

$$Q = A \exp\left[-\frac{4(x^2 + y^2)}{R_I^2} \right]. \tag{2.5}$$

Hence the injection rate I is related with the injection amplitude A and the radius R_I as follows

$$I = \int Q dS = 2\pi A \int_0^\infty \exp\left[-\frac{4r^2}{R_I^2} \right] r dr = \frac{\pi}{4} A R_I^2.$$

Our idealized ocean has two internal deformation radii $R_\pm$, where subscripts + and − denote first and second baroclinic mode respectively. Those are given by

$$R_\pm \equiv \left[\frac{F_1 + F_2 + F_3 \mp \sqrt{(-F_1 + F_2 + F_3)^2 + 4F_1F_2}}{2} \right]^{-1/2}, \tag{2.6}$$

where

$$F_1 = f_0^2/(g_{um}H_u), \quad F_2 = f_0^2/(g_{um}H_m), \quad F_3 = f_0^2/(g_{ml}H_m),$$

and H_i, $(i=u,m)$ are the undisturbed layer thicknesses. If the upper layer thickness becomes infinity, the second baroclinic radius R_- is reduced to the deformation radius R_d [$\equiv (F_2+F_3)^{-1/2}$] of an equivalent barotropic model with only an intermediate layer in motion. Since the intermediate layer is assumed to be thin, the inequality $H_u \gg H_m$ is always satisfied as illustrated in Figure 1. Therefore R_d and R_- are very much alike.

Using R_d instead of R_- as the horizontal length scale and $1/f_0$ as the timescale, we nondimensionalize variables as follows

$$t^* = (1/f_0^*)t, \; x^* = R_d^* x, \; \hat{\mathbf{u}}^{i*} = R_d^* f_0^* \hat{\mathbf{u}}^i, \; h^{i*} = H_i^* h^i, \; Q^* = H_m^* f_0^* Q,$$

where dimensional variables are denoted with an asterisk. Note that both h^u and h^m are normalized independently to make the undisturbed thickness unity. Introducing Kronecker's delta δ_{ij}, we obtain nondimensionalized equations:

$$\frac{D\hat{\mathbf{u}}^i}{Dt} + (1+\beta y)\hat{\mathbf{z}} \times \hat{\mathbf{u}}^i = -\nabla p^i - \delta_{im}\frac{Q}{h^m}\hat{\mathbf{u}}^m, \tag{2.7}$$

$$\frac{\partial h^i}{\partial t} + \nabla\cdot(\hat{\mathbf{u}}^i h^i) = \delta_{im} Q, \tag{2.8}$$

where p^i, $(i=u,m)$ are the hydrostatic pressure anomalies given by

$$p^u = (1+\gamma)\delta h^u + \left(1+\frac{1}{\gamma}\right)(\delta h^u + h^m), \quad p^m = \left(1+\frac{1}{\gamma}\right)(\delta h^u + h^m), \tag{2.9}$$

and three nondimensional parameters are defined by

$$\beta = \frac{R_d^*}{f_0^*}\beta^*, \quad \gamma = \frac{g_{um}^*}{g_{ml}^*}, \quad \delta = \frac{H_u^*}{H_m^*}. \tag{2.10}$$

We introduce the potential vorticity q^i in each layer for the future convenience as follows

$$q^i = \frac{\zeta^i + 1 + \beta y}{h^i}, \tag{2.11}$$

where $\zeta^i = \hat{\mathbf{z}} \cdot \nabla \times \hat{\mathbf{u}}^i$ denote the relative vorticity. Furthermore, we introduce vertical modes defined as

$$(u^{\pm}, v^{\pm}, h^{\pm}) = (u^u, v^u, h^u) + \tau_{\pm}(u^m, v^m, h^m), \tag{2.12}$$

where $\tau_{\pm}$ are given by

$$\tau_{\pm} = \frac{-(-1 + \delta + \delta\gamma) \pm \sqrt{(-1 + \delta + \delta\gamma)^2 + 4\delta}}{2\delta}. \tag{2.13}$$

From (2.9) we have the relation

$$p^u + \tau_{\pm} p^m = R_{\pm}^2 (h^u + \tau_{\pm} h^m). \tag{2.14}$$

3. NUMERICAL EXPERIMENT

3.1. Model Description

We assume the following dimensional values on the basis of observations in the mid-latitude region of the North Pacific:

$$H_u^* = 1000\,\text{m}, \quad H_m^* = 300\,\text{m},$$
$$\rho_u^* = 25.2\ \sigma_\theta, \quad \rho_m^* = 26.7\ \sigma_\theta, \quad \rho_l^* = 27.4\ \sigma_\theta,$$

where ρ_m^*, expressed using the sigma-theta here, corresponds to the typical density of the NPIW. With the above stratification as well as the planetary parameters evaluated at 30°N, the two relevant internal deformation radii are given by

$$R_+^* = 63.8\,\text{km}, \quad R_-^* = 15.8\,\text{km}, \quad (\text{where } R_d^* = 16.0\,\text{km}), \tag{3.1}$$

or

$$R_+ = 3.98, \quad R_- = 0.984, \quad \text{(where } R_d = 1 \text{ as defined)}, \qquad (3.2)$$

without dimension. Since R_d^* is adopted as a lateral length scale, the β-parameter is given by 4.3×10^{-3}. We note that the long Rossby wave speed for the second baroclinic mode (given by $-\beta R_-^2$) is almost the same with the equivalent barotropic mode (given by $-\beta R_d^2$) in the present situation. This is because the upper layer is much thicker than the intermediate layer.

Numerical integration of (2.7)–(2.8) is carried out using a finite difference scheme based on Arakawa and Lamb (1981). The domain is given by $150\,R_d \times 50\,R_d$ (about 2400 km × 800 km) in the x and y directions with grid spacing of $1.25\,R_d$. The model is periodic in the x direction; sponge layers (of which width is $3.75\,R_d$) are introduced near the northern and southern walls to erase unnecessary wave reflection. The conventional biharmonic viscosity is adopted to guarantee numerical stability. The model is integrated for 1000 days from the initial condition of no motion (*i.e.*, $h^i = 1$ and $\hat{u}^i = 0$, for $i = u, m$) keeping a constant injection rate I^* ranging from 1.0×10^{-2} Sv to 1.0 Sv, where the injection radius R_I is fixed at $3.0\,R_d$.

Hereafter, we will refer to the injection rate I^* [Sv] (the integral time t^* [day]) in a dimensional manner, because it enable us to compare our results directly with observations. We note here that $I^* = 1.0$ Sv ($t^* = 1000$ day) corresponds to $I = 0.179$ ($t = 2\pi \times 10^3$) in a non-dimensional form.

3.2. Three Regimes on a β-plane

It has turned out that the oceanic response is classified into three categories based on the injection rate I^*(Sv). Those are the Rossby wave regime (for $I^* < 5.0 \times 10^{-2}$ Sv), the weakly nonlinear regime (for 5.0×10^{-2} Sv $< I^* < 8.0 \times 10^{-2}$ Sv) and the strongly nonlinear regime (for $I^* > 8.0 \times 10^{-2}$ Sv) as summarized in Table I. One of clear differences between the Rossby wave regime and the weakly nonlinear regime is the vortex shedding. In transition from the weakly nonlinear regime to strongly nonlinear regime, the westward migration speed of eddies increases dramatically and the

TABLE I Summary of numerical results in typical three regimes. Minimum value of h^u, maximum value of the h^m, and minimum values of the ζ^u and ζ^m at day 1000 are shown for $I^* = 1.0 \times 10^{-2}$ Sv, 5.6×10^{-2} Sv and 1.0 Sv. Ω^u and Ω^m denote rotation rates, *i.e.*, Rossby number near the center of vortices in the upper and middle layer, respectively.

$I^*(Sv)$	$h^u\|_{min}$	$h^m\|_{max}$	$\zeta^u\|_{min}(=2\Omega_u)$	$\zeta^m\|_{min}(=2\Omega_m)$
1.0×10^{-2}	0.99	1.10	−0.0012	−0.027
5.6×10^{-2}	0.97	1.37	−0.022	−0.083
1.0	0.90	2.72	−0.068	−0.19

upper layer potential vorticity q^u shows closed contours, suggesting strong coupling between the first and second baroclinic modes.

3.2.1. Rossby Wave Regime ($I^* \leq 5.0 \times 10^{-2}$ Sv)

When the injection rate is sufficiently small, the response is essentially wavelike (Fig. 2). The X-T diagram for the evolution of the intermediate layer thickness h^m shows clearly that linear long Rossby waves are excited as expected. The injected water actually spreads to the west with its front traveling westwards almost exactly at the second baroclinic long Rossby wave speed $-\beta R_2^2$ (Figs. 2a, b). The upper layer potential vorticity q^u is dominated by the undisturbed value $1+\beta y$ (Fig. 2c) as expected from the weak modulation of the interface (Fig. 2d). This is consistent with Figure 3, in which the first baroclinic component is more dispersed away than the second baroclinic component. The above suggests that conventional linear QG potential vorticity dynamics subject to vertical modal decomposition works well in this regime (Longuet-Higgins, 1965; Davey and Killworth, 1989).

3.2.2. Weakly Nonlinear Regime (5.0×10^{-2} Sv $\leq I^* \leq 8.0 \times 10^{-2}$ Sv)

Increasing the injection rate leads to shedding of weakly nonlinear vortices (Fig. 4). The q^m-field shows closed contours clearly. However, those vortices are not fully isolated each other; they are attached to neighboring vortices (Fig. 4b). Although the q^u-field does not show closed contours, a region of uniform potential vorticity appears just above the vortex in the intermediate layer (Fig. 4c). Figure 5

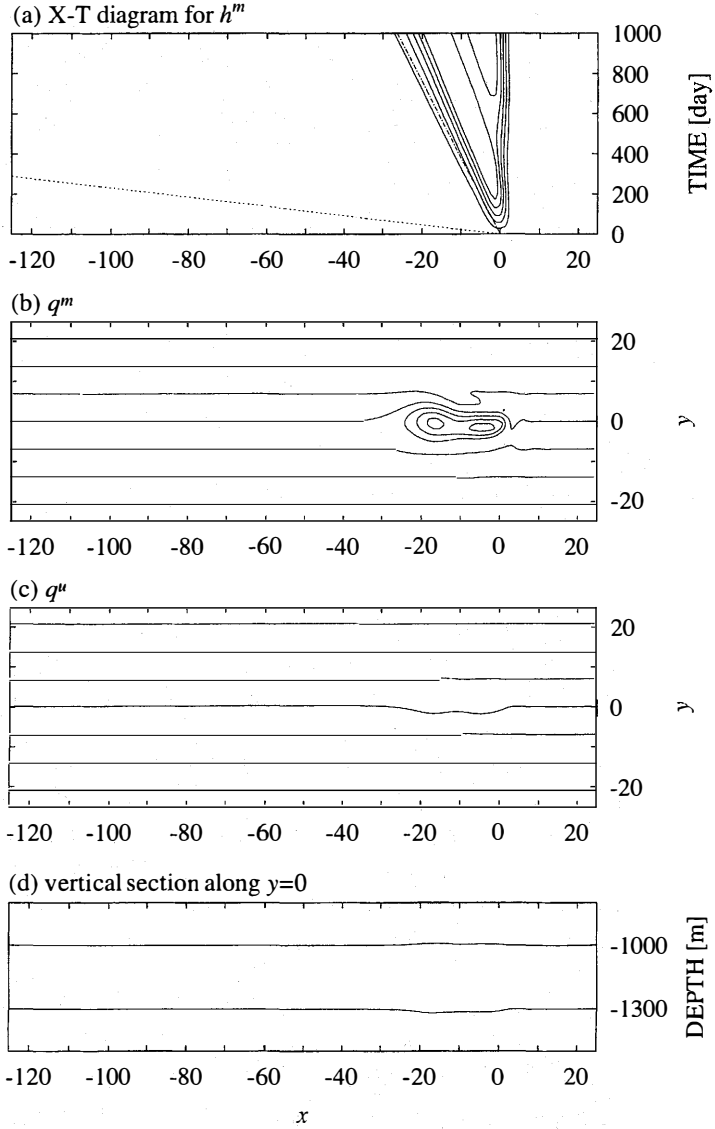

FIGURE 2 Solution for $I^* = 1.0 \times 10^{-2}$ Sv at day 1000. The dashed (dot-dashed) line denotes the phase speed of the first-(second) baroclinic long Rossby wave. (a) Evolution of the intermediate layer thickness h^m. (b) The spatial distribution of q^m. (c) The spatial distribution of q^u. (d) Vertical section along $y=0$. The horizontal coordinates (x, y) are nondimensionalized using R_d^*. Contour interval is 0.015 for (a), 0.03 for both (b) and (c).

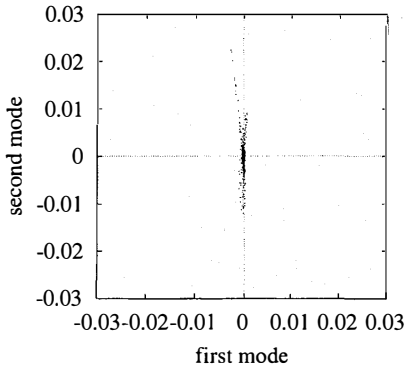

FIGURE 3 Modal decomposition of the meridional velocity at all grid points in the upper and intermediate layer (v^u, v^m) at day 1000 for $I^* = 1.0 \times 10^{-2}$ Sv. The *abscissa* (or ordinate) denotes the projection of the (v^u, v^m) onto the unit base of the first (or second) baroclinic mode $(1, \tau_+)/|(1, \tau_+)|$ [or $(1, \tau_-)/|(1, \tau_-)|$]. The normal basis are calculated at every grid point using the ratio of the upper and intermediate layer thickness $\delta(= h^{u*}/h^{m*})$.

shows the disappearance of pure second baroclinic waves, although contribution from the second baroclinic component is still dominant. The vortices which are composed of coupled vertical modes travel westward faster than the second baroclinic long Rossby wave, but slower than the first baroclinic long Rossby wave (Fig. 4a).

Evolution of the potential vorticity field in the intermediate layer is shown in Figure 6, which demonstrates how weakly nonlinear vortices are shed. The injected water initially spreads around the source and then forms anticyclones successively. Nonlinearity due to the increase of h^m, together with the weak coupling between the first baroclinic mode and the second baroclinic mode, enables the vortex to travel westward faster than the second baroclinic linear long Rossby wave (*cf.* Yamagata, 1982). As the eddy moves farther away from the source region, the forcing again starts generating low q^m, forming another vortex.

3.2.3. Strongly Nonlinear Regime ($I^* \geq 8.0 \times 10^{-2}$ Sv)

When the injection rate I^* is increased up to 1.0 Sv, anticyclonic lenses with large amplitude are shed regularly (Fig. 7, see also Tab. I). Those lenses travel westward with a speed several times faster than the second baroclinic long Rossby wave speed (Fig. 7a). The

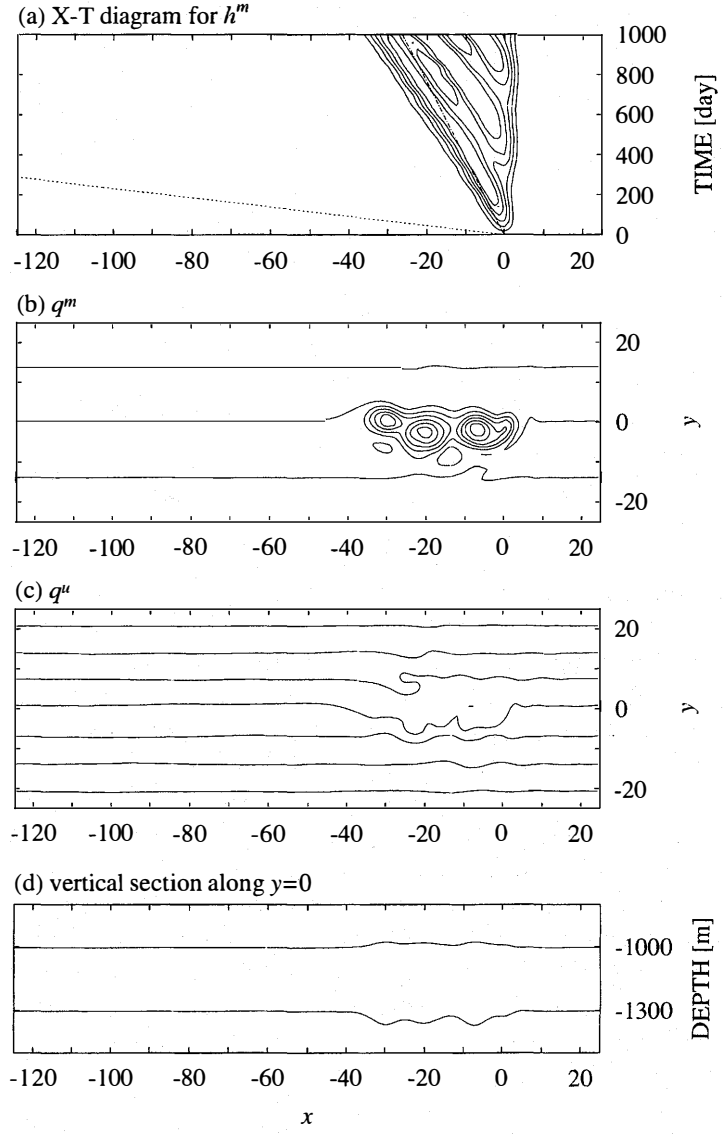

FIGURE 4 Same as Figure 2 except for $I^* = 5.6 \times 10^{-2}$ Sv. Contour interval is 0.06 for both (a) and (b), and 0.03 for (c).

rotation rates near the core in both layers are almost comparable, this strong spin in the upper layer creates the closed q^u-contours above those in the intermediate layer (Figs. 7b, c). The time evolution of

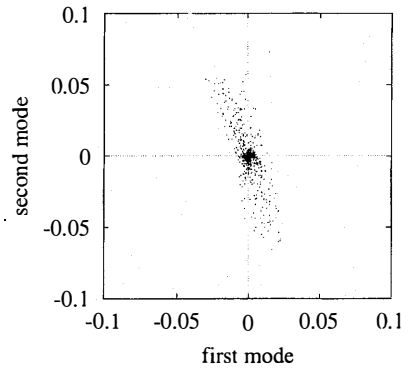

FIGURE 5 As in Figure 3 except for $I^* = 5.6 \times 10^{-2}$ Sv.

lenses shown in Figure 8 demonstrates the following characteristics: (i) lenses are almost axis-symmetric and separated each other; (ii) they propagate much faster than vortices in the weakly nonlinear regime; (iii) the radius of lenses is much larger than that in the weakly nonlinear regime.

As shown in Figure 9, the first baroclinic component is strengthened compared with that in Figure 5. This contribution mostly comes from the vortex interior. It is also associated with negative ζ^u arising from the larger modulation of the interface with q^u conserving its initial value. The first baroclinic component is thus almost frozen inside the vortex and cannot be dispersed away as free first baroclinic Rossby waves. We note, however, clear presence of dots along the *abscissa* around origin in Figure 9. Although this shows the existence of radiation of first baroclinic Rossby waves; those radiative waves, mostly associated with positive anomalies of h^u, are actually found north of the subsequently generated vortices rather than the westernmost vortex generated initially (Fig. 7c).

4. TRANSLATION SPEED OF LENSES IN THE INTERMEDIATE LAYER

4.1. Euler's Momentum Integral Theorem

In Figure 10, we have plotted the observed translation speed as a function of the injection rate I^*. The speed is almost constant in the

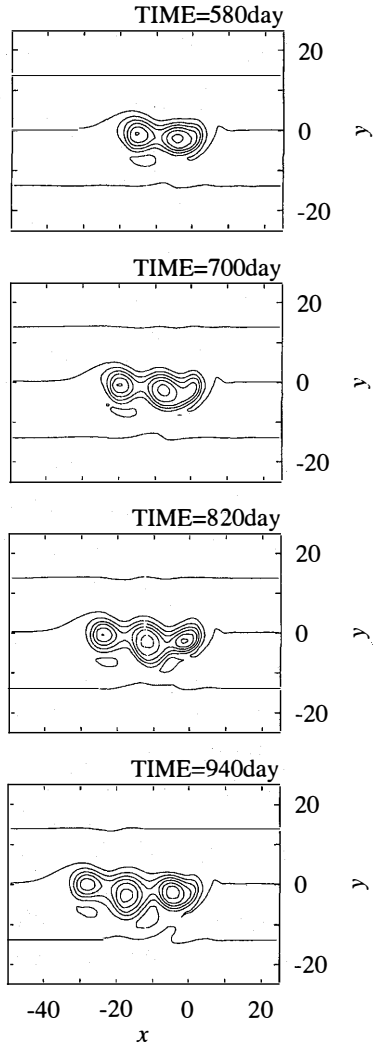

FIGURE 6 Evolution of the potential vorticity in the intermediate layer for $I^* = 5.6 \times 10^{-2}$ Sv. Time interval is 120 days. Contour interval is 0.06.

Rossby wave regime as is expected from the linear theory. It increases dramatically within the nonlinear regime. In particular, the translation speed in the strongly nonlinear regime is several times larger than the second baroclinic long Rossby wave speed $-\beta R_2^2$ (which is about unity in the ordinate of Fig. 10).

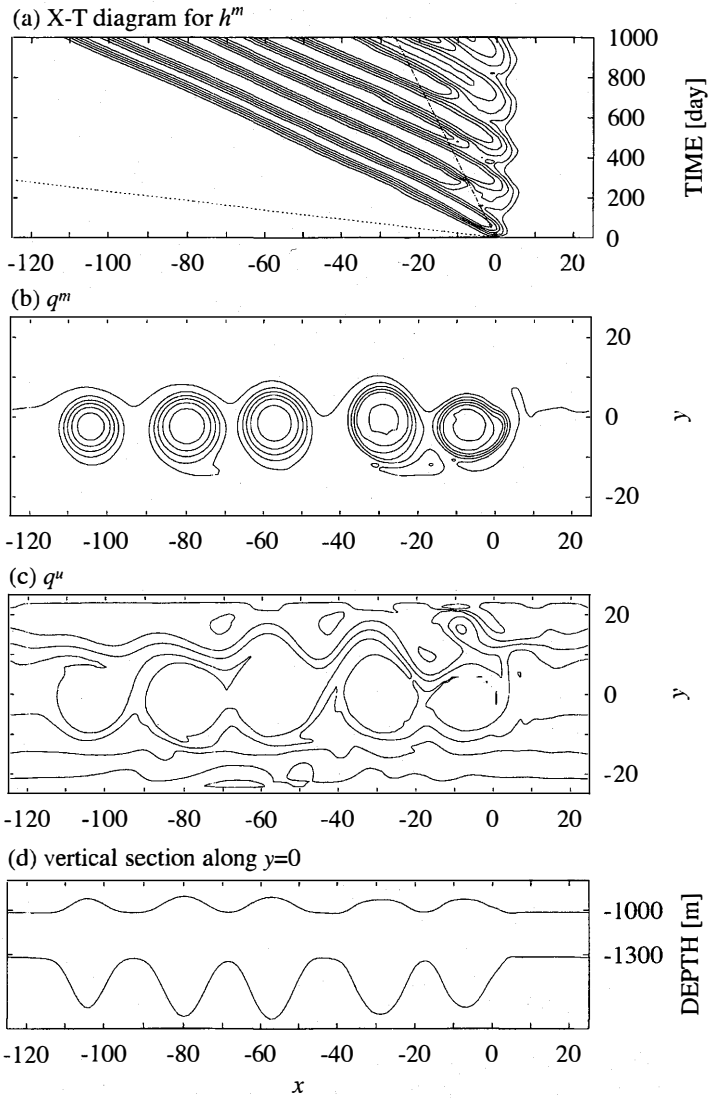

FIGURE 7 As in Figure 2 except for $I^* = 1.0$ Sv. Contour interval is 0.3 for (a), 0.12 for (b) and 0.03 for (c).

In this subsection, using the Euler's momentum integral theorem, we study more details on the translation speed of the isolated baroclinic vortices. The theorem itself has a long history in fluid

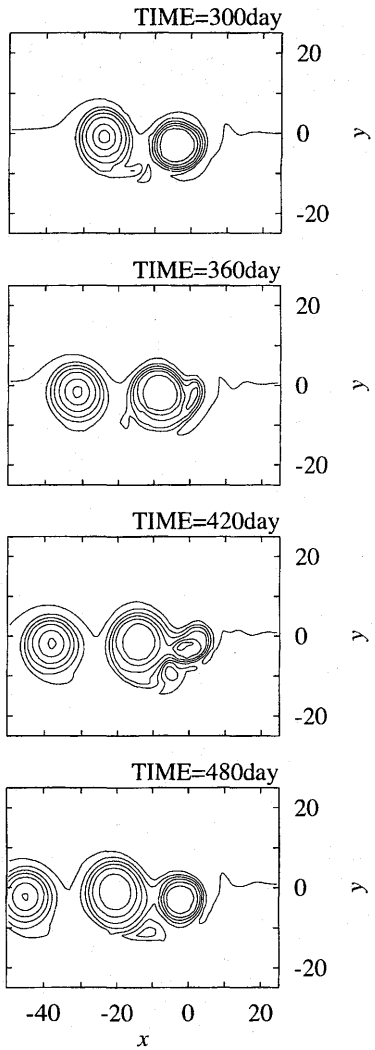

FIGURE 8 Evolution of the potential vorticity in the intermediate layer for $I^* = 1.0$ Sv. Time interval is 60 days. Contour interval is 0.12.

dynamics. However, it was introduced by Nof (1981) and Killworth (1983) in geophysical fluid dynamics in order to derive a translation speed for equivalent barotropic vortices. Then Nof (1985) and Cushman-Roisin *et al.* (1990) applied the theorem to baroclinic vortices.

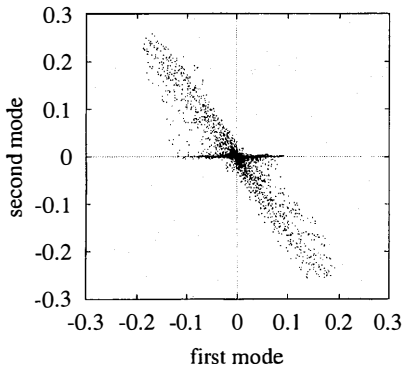

FIGURE 9 As in Figure 3 except for $I^* = 1.0$ Sv.

If the volume anomaly of the intermediate layer is given by M, the center $\hat{\mathbf{X}} = [X, Y]$ of the intermediate lens is defined by

$$\hat{\mathbf{X}} = \int (h^m - 1)\hat{\mathbf{x}} dS/M,$$

where the integral area covers all anomalous field of h^m. In order to high-light the difference between the 1.5-layer model and the present 2.5-layer model, we first review the solution for the translation speed in the 1.5-layer model. The limit of no motion in the upper layer in the present model corresponds to the 1.5-layer model; assuming $\nabla p^u = \mathbf{0}$ in (2.9) leads to $\nabla p^m = \nabla h^m$. Using the same manner as in Killworth (1983), we obtain the translation speed for the 1.5-layer vortex with radial symmetry as follows,

$$X_t = -\beta E_0/M_0, \tag{4.1}$$

$$Y_t = 0, \tag{4.2}$$

where the subscript 0 denotes the leading order of β. The quantity E_0 in the above expression is a surface integral

$$E_0 = \int \left(\int_{\infty}^{r} h_0^m V_0^m dr \right) dS, \tag{4.3}$$

where V_0^m denotes azimuthal velocity. In the 1.5-layer model, E_0 is simply reduced to the sum of the nondimensional volume anomaly,

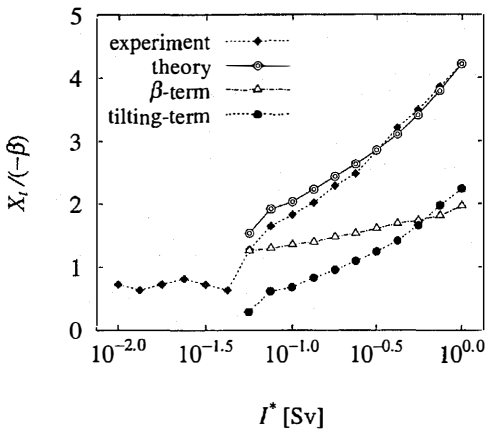

FIGURE 10 Zonal translation speed (normalized using the equivalent barotropic long Rossby wave speed $-\beta$) as a function of injection rate I^*. The closed diamond denotes the experimental results (calculated simply by tracking the maximum h^m from day 500 to day 1000). The double circle denotes the theoretical estimate based on (4.5) using the results at day 1000. The open triangle and closed circle denote the β-term and the tilting-term on the right hand side of (4.5).

net kinetic energy and net available potential energy:

$$E_0 = M_0 + 2\pi \int \frac{1}{2}[h_0^m V_0^{m2} + (h_0^m - 1)^2] r dr. \tag{4.4}$$

If both total energy and volume anomaly are conserved, the zonal translation speed is constant. Since the azimuthal velocity V_0^m is directly related to h_0^m according to the cyclostrophic balance: $h_{0r}^m = V_0^m + V_0^{m2}/r$, we can calculate the translation speed once either V_0^m or h_0^m is known. We note that the $\mathcal{O}(\beta)$ field has no contribution to the translation speed in a 1.5-layer model. We have completely neglected the contribution from inertial oscillations. It is easy to see that anticyclones travel westward faster than the equivalent barotropic long Rossby wave because of the inequality $E_0 > M_0 > 0$ (*cf.* Yamagata, 1982; Matsuura and Yamagata, 1982). For cyclones, however, the translation speed lies within the subcritical range ($-\beta < X_t < 0$) because M_0 is negative.

Applying a similar method to the 2.5-layer model leads to a formula for more general baroclinic vortices; readers are referred to Cushman-Roisin *et al.* (1990) in this context. The major difference from (4.1) and (4.2) is that the 2.5-layer version contains additional

terms as follows

$$X_t = -\beta E_0/M_0 - \left(1+\frac{1}{\gamma}\right)\delta W^y/M_0, \tag{4.5}$$

$$Y_t = \left(1+\frac{1}{\gamma}\right)\delta W^x/M_0. \tag{4.6}$$

The additional terms depend on the structure of the $\mathcal{O}(\beta)$ field if expanded as $h^i(r,\theta) = h_0^i(r) + \beta\tilde{h}_1^i(r)\sin\theta + \beta\hat{h}_1^i(r)\cos\theta$, $(i = u, m)$. Those are given explicitly in the following:

$$W^x = \int (h^m - 1)\frac{\partial h^u}{\partial x}dS = \beta\pi\int (h_{0r}^u\hat{h}_1^m - h_{0r}^m\hat{h}_1^u)rdr + \mathcal{O}(\beta^2), \tag{4.7}$$

$$W^y = \int (h^m - 1)\frac{\partial h^u}{\partial y}dS = \beta\pi\int (h_{0r}^u\tilde{h}_1^m - h_{0r}^m\tilde{h}_1^u)rdr + \mathcal{O}(\beta^2). \tag{4.8}$$

Some qualitative analyses have been reported so far on the role of the additional terms for the translation of the isolated baroclinic vortex (Flierl, 1984; Nof, 1985; Killworth, 1986; Cushman-Roisin *et al.*, 1990; Pakyari and Nycander, 1996). In particular, Nof (1985) derived the following simple relation by assuming the exact cancelation between contributions from the upper and intermediate layers. In other words, he assumed the existence of an isolated vortex coherent in both layers and derived

$$X_t = -\beta\int (\delta h_0^u V_0^u + h_0^m V_0^m)r^2dr \Big/ \iint (\delta h_{0r}^u + h_{0r}^m)r^2dr, \tag{4.9}$$

$$Y_t = 0. \tag{4.10}$$

The above relation is useful for clarifying the role of the additional terms arising from interaction between the upper and the intermediate layer. If it were not for interaction between the upper layer vortex and the intermediate layer vortex, each vortex could translate separately according to its own β-term (*i.e.*, the first term on the right-hand side of (4.5)). Since the interaction allows vortices to move coherently, the difference of each zonal translation speed must be mediated somehow by a meridional pressure gradient force giving rise to an additional

zonal flow. This explains the existence of the second term (so-called tilting-term) of (4.5).

Another way to understand the tilting-term is to consider the perturbation layer thickness arising from the β-effect. A water column on the closed streamline must be stretched (squeezed) in the northern (southern) half in order to conserve its potential vorticity. As a result, both upper and intermediate layer vortex involves positive (negative) anomaly of the layer thickness in the northern (southern) half ($\tilde{h}_1^u$, $\tilde{h}_1^m > 0$, see Fig. 11). Taking into account that $h_{0r}^u > 0$ and $h_{0r}^m < 0$ in (4.8), we find that the meridional asymmetry of the perturbation layer thickness always make W^y positive, indicating additional westward translation. In other words, the slight northward increase of the upper layer thickness just above the intermediate vortex provides a kind of topographic β-effect giving rise to additional westward translation; we note from (4.8) that uniform meridional gradient of the upper layer thickness may contribute an additional constant value to the phase speed just like the topographic Rossby wave (*cf.* Nof, 1983).

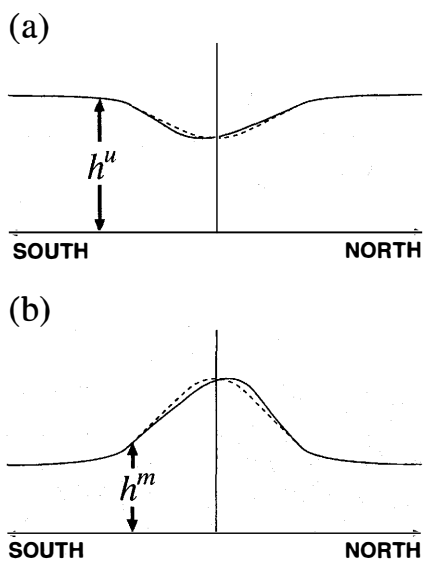

FIGURE 11 Schematic picture of the layer thickness along the meridional section crossing the center of the vortex; (a) upper layer and (b) intermediate layer. The solid line depicts the layer thickness including $\mathcal{O}(\beta^1)$ field. The dashed line shows the leading order layer thickness of β for comparison.

Figure 12 actually shows that the upper layer vortex lies slightly south of the intermediate layer vortex, which confirms the meridional asymmetry of the perturbation layer thicknesses. This vertical tilt, which is the origin of the tilting-term, is also consistent with the general feature of baroclinic flows on a β-plane, the so-called beta spiral. This important concept for planetary stratified flows was originally introduced by Sudo (1965) and later developed by Stommel and Schott (1977) to determine absolute geostrophic flows in the ocean. This explains the tilting pattern quite well from the Lagrangian perspective as illustrated in Figure 13. Let us consider, southward (northward) movement of a column in the intermediate layer vortex, which must be associated with decrease (increase) of the intermediate layer thickness along its trajectory in order to conserve f/h. Since the interface between the intermediate layer and the lower layer is kept at a constant depth along the trajectory, the interface between the upper and the intermediate layer must slope downward

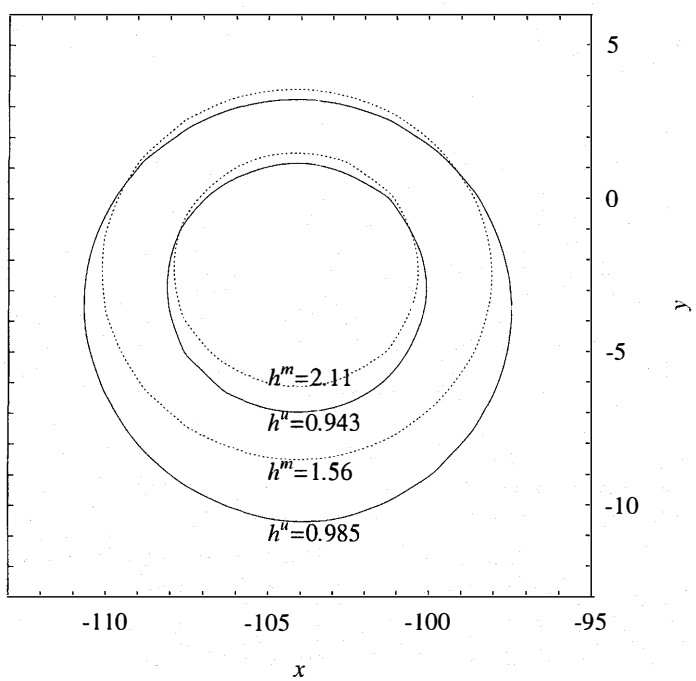

FIGURE 12 Contours of h^u and h^m for the most western vortex in Figure 7.

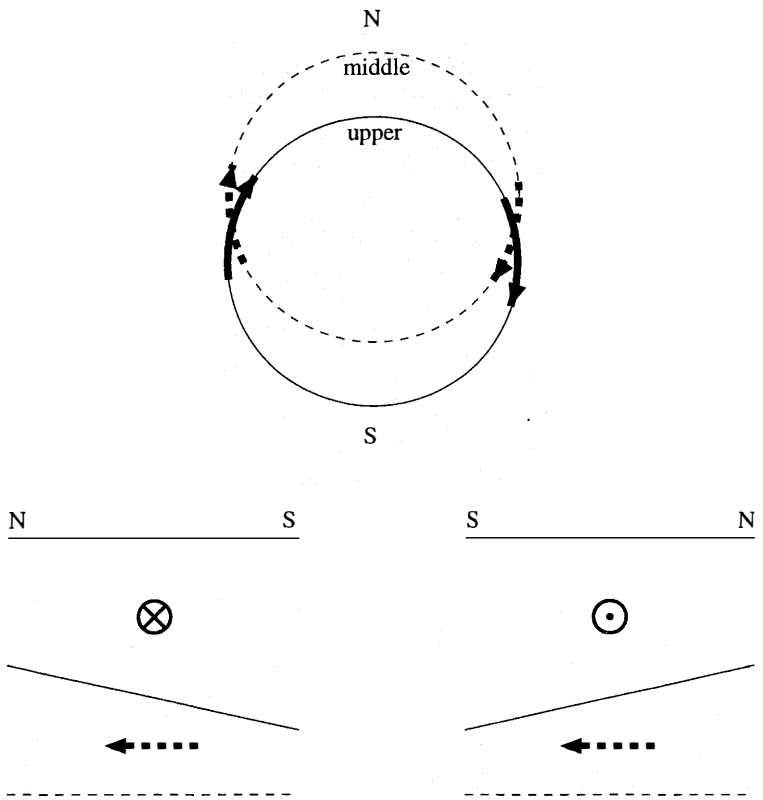

FIGURE 13 A schematic view of the beta spiral in the 2.5 layer vortex. Upper figure illustrates streamlines in both upper and intermediate layers. Lower right (left) figure shows vertical section along the eastern (western) half of the intermediate streamline, seen from the outside of the vortex. Southward (northward) movement in the intermediate layer must be associated with decrease (increase) of the intermediate layer thickness to conserve f/h in planetary geostrophic dynamics. As a result, the eastward (westward) flow component appears in the upper layer, crossing the streamline in the intermediate layer. Thus velocity vector spirals clockwise (anticlockwise) with increase of depth.

(upward) in the direction of the column movement. This interface slope is associated with the geostrophic eastward (westward) flow component in the upper layer, crossing the streamline in the intermediate layer. Consequently, a baroclinic vortex on a β-plane involves inevitably vertical tilt in the meridional direction as shown in Figure 13. The existence of anticyclones slightly shifted between upper and intermediate layers, together with the negative anomaly of h^u

and the positive anomaly of h^m, thus explains the tilting-term providing the additional translation speed for the monopole in the intermediate layer. The root cause of the additional term lies in the baroclinicity of a planetary vortex.

Figure 10 compares the zonal translation speed estimated from the experiments with the formula given by (4.5). We see that the theory predicts the numerical results quite well. Contributions from the β-term and the additional tilting-term are also shown in the same figure. We note that the contribution from the tilting-term becomes comparable to that from the β-term with increasing the injection rate. This verifies that the upper layer movement significantly influences the translation of the intermediate lens.

The origin of the meridional translation given by (4.6) is also understood in a similar way. The existence of slight zonal shift of the upper layer vortex may provide an additional meridional translation speed of the intermediate layer vortex due to a kind of topographic β-effect. As seen in Figure 12, however, the zonal shift is quite small in the present situation. This is reasonable because there is no reason for generating the zonal shift in the structure of the $\mathcal{O}(\beta)$ field for an axis-symmetric vortex in a baroclinic planetary fluid.

4.2. A Dispersion Relation

Here we discuss the translation of the isolated baroclinic vortex from a viewpoint different from the Euler's momentum integral theorem. We derive a dispersion relation, which relates the vortex radius to the translation speed, using a steady nonlinear solution for the QG potential vorticity equation. The present approach is partially similar to the well-known Modon theory (*cf.* Flierl *et al.*, 1980).

The periphery of the vortex, where Rossby number is as small as the β-parameter, may be governed by the QG dynamics, although the vortex interior needs another approximation due to the large amplitude of layer thicknesses (see Fig. 7d). Thus, the outer field is reasonably governed by

$$J[p^i - p^i|_{h^u=h^m=1} + c\beta y, \nabla^2 p^i - (h^i - 1) + \beta y] = 0, \quad (i = u, m \text{ and } c = X_t/\beta). \tag{4.11}$$

Here we have also assumed the steady zonal translation of the vortex over a suitable time span. The QG potential vorticity equation is reduced to

$$\nabla^2 p^i - (h^i - 1) + \beta y = F(p^i - p^i|_{h^u=h^m=1} + c\beta y), \tag{4.12}$$

where F is an undetermined functional. The functional F can be determined by considering a localized phenomenon as well as taking the limit $h^i \to 1, (i=u,m)$ in the infinity. This yields $F(y)=y/c$. Therefore we obtain

$$\nabla^2 p^i - (h^i - 1) = \frac{1}{c}(p^i - p^i|_{h^u=h^m=1}). \tag{4.13}$$

If the variables are decomposed into the vertical normal modes defined in (2.12), we obtain the following Bessel equation:

$$\nabla^2 h^{\pm} - \left(\frac{1}{R_{\pm}^2} + \frac{1}{c}\right)(h^{\pm} - h^{\pm}|_{h^u=h^m=1}) = 0. \tag{4.14}$$

The equation is written more explicitly for the radially symmetric case,

$$V_{rr}^{\pm} + \frac{1}{r}V_r^{\pm} - \left(\kappa_{\pm}^2 + \frac{1}{r^2}\right)V^{\pm} = 0, \quad \kappa_{\pm}^2 = \frac{c + R_{\pm}^2}{cR_{\pm}^2}, \tag{4.15}$$

where $h_r^{\pm}$ is replaced by azimuthal velocity $V^{\pm}$. Since our numerical results show $-R_+^2 < c < -R_-^2$, we expect that the first baroclinic mode consists of an oscillating solution such as $V^+(r)=J_1(\kappa_+ r)$. Therefore, we assume the structure near the periphery of the vortex as

$$\begin{aligned} V^+ &= J_1(\kappa_+ r), \quad (\kappa_+ r < 3.8), \\ V^+ &= 0, \quad (\kappa_+ r \geq 3.8), \end{aligned} \tag{4.16}$$

where $\kappa_+ r = 3.8$ is the gravest zero point of $J_1(\kappa_+ r)$. Thus we obtain a dispersion relation, which relates the vortex radius R to the migration

speed c, such as

$$R = 3.8\sqrt{\frac{cR_+^2}{c + R_+^2}}. \tag{4.17}$$

It is rather amazing that the above simple dispersion relation explains the numerical results quite well for a wide range of the injection rate, as displayed in Figure 14. On deriving the dispersion relation, we have used the boundary condition allowing the velocity discontinuity around the monopole vortex. This contrasts with the traditional Modon theory in which the velocity continuity around the boundary of the dipole is satisfied for the first azimuthal mode (*cf.* Stern, 1975).

As seen in Figure 7, we note the westernmost vortex has the smallest radius among the five vortices. The same is true for all cases in the strongly nonlinear regime (not shown). Hence the disagreement between the theory and the numerical results is mostly associated with the vortices generated subsequently. In other words, the dispersion relation (4.17) may involve an error for those subsequent vortices

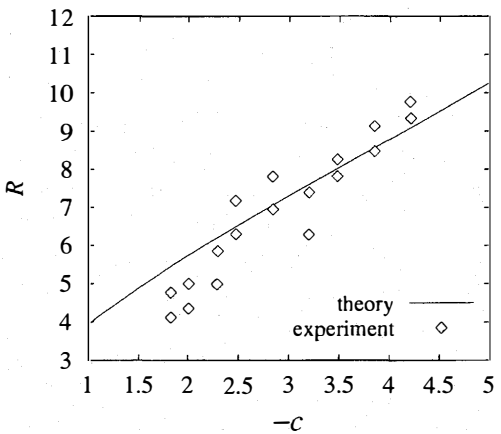

FIGURE 14 Relation between the westward translation speed and radius of vortices. The open diamonds denote the relation derived from the experiments for $I^* =$ 0.10, 0.13, 0.18, 0.24, 0.32, 0.42, 0.56, 0.75 and 1.0 Sv; we have selected only the westernmost two vortices. The solid line denotes the theoretical dispersion relation given by (4.17).

which are associated with more complicated structure in the outer field than the westernmost vortex generated initially (see Section 3.2.3.).

5. SUMMARY AND DISCUSSION

The dynamics related to the formation of those intermediate water lenses has been discussed in detail in the present article from the viewpoint of geophysical fluid dynamics. Numerical experiments with idealized injection of intermediate water mass in the 2.5-layer ocean model have shown three different regimes of dynamical response depending on the forcing magnitude.

The weak forcing generates linear long Rossby waves as expected. Increasing the forcing leads to shedding of weakly nonlinear vortices which propagate westward. When the injection rate is increased up to 1.0 Sv, isolated lenses associated with strong anticyclonic circulation are shed successively. The lenses show strong baroclinicity and travel westward several times faster than the second baroclinic long Rossby wave. Such formation of highly nonlinear vortices is very different from the similar experiment of Davey and Killworth (1989) using the 1.5-layer model with limited baroclinicity and thus demonstrates the existence of a new dynamical regime. For example, in Figure 9 of Davey and Killworth (1989), the injection rate of $I=$ 0.17 Sv (which corresponds to $1.26 \times 10^{-3} HR_d^2 f$ with $H = 1000$ m and $R_d = 42.9$ km) leads to shedding of weakly nonlinear eddies whose amplitude is $1.043\,H$; they also report that further increase in forcing amplitude yields a completely unsteady response. In contrast with this, our experiment shows the successive formation of intense vortices similar to lenses, whose amplitude is $2.72\,H_m$ when the injection rate is $I = 1.0$ Sv (which corresponds to $0.179\,H_m R_d^2 f$ with $H_m = 300$ m and $R_d = 16.0$ km).

The Euler's momentum integral theorem has revealed that the fast westward translation is due to a kind of topographic β-effect associated with the induced upper-layer vortex. The meridional shift of the induced vortex confirms this mechanism. Assuming quasi-geostrophy in the outer field, a simple dispersion relation determining the translation speed as a function of the lens radius is derived. It is found that the relation predicts the numerical results amazingly well. This relation also indicates that the fast westward translation

is associated with the first baroclinic component of the azimuthal flow. It is important to note that the above properties are derived from a general nature of baroclinic flow *on a planetary β-plane*, whereas baroclinic vortices generated *on a sloping bottom* in a rotating tank must be classified into a different category.

We are successful in reproducing the ubiquitous lenses as observed in the intermediate layer using a relatively simple model. However, the shedding mechanism remains unanswered even if the fast translation as well as the highly nonlinear advection may partly explain the separation. The injection rate around 0.1 – 1.0 Sv has led to the successive formation of intense lenses in our results. This is consistent with the observed range for the local convection, such as the volume transport of Mediterranean outflow and the formation rate of the NPIW. The core rotation rate of the vortices observed in our strongly nonlinear regime ranges from $0.05f$ to $0.1f$, and the diameter is from 130 km to 320 km. As shown in the introduction, however, the SCVs observed in the real ocean show more nonlinear behavior compared to the vortices in the present work. We suggest that less nonlinearity of our results may be due to relatively thick intermediate layer (= 300 m). If we allow the intermediate layer vanish in the outer field, the theoretical constraint suggested by Pichevin and Nof (1997) and Nof and Pichevin (1996) could be applicable in a more general form. Further work is certainly needed to explore this interesting lens formation.

Acknowledgments

This article is dedicated to the late Dr. M. Nezlin who dedicated the latter half of his life to nonlinear eddy dynamics in planetary fluids. We also thank Drs. A. Zatsepin and N. Maximenko for their consistent support of the present work. H. A. was supported by the Research Fellowships of the Japan Society for the Promotion of Science for Young Scientists.

References

Arakawa, A. and Lamb, V. R., "A potential enstrophy and energy conserving scheme for the shallow water equations," *Mon. Wea. Rev.* **109**, 18 – 36 (1981).

Armi, L. and Zenk, W., "Large lenses of highly saline Mediterranean Water," *J. Phys. Oceanogr.* **14**, 1560 – 1576 (1984).

Cenedese, C. and Linden, P. F., "Cyclone and anticyclone formation in a rotating stratified fluid over a sloping bottom," *J. Fluid Mech.* **381**, 199–223 (1999).
Cushman-Roisin, B., Chassignet, E. P. and Tang, B., "Westward motion of mesoscale eddies," *J. Phys. Oceanogr.* **20**, 758–768 (1990).
Davey, M. K. and Killworth, P. D., "Flows produced by discrete sources of buoyancy," *J. Phys. Oceanogr.* **19**, 1279–1290 (1989).
Flierl, G. R., "Rossby wave radiation from a strongly nonlinear warm eddy," *J. Phys. Oceanogr.* **14**, 47–58 (1984).
Flierl, G. R., Larichev, V. D., McWilliams, J. C. and Reznik, G. M., "The dynamics of baroclinic and barotropic solitary eddies," *Dyn. Atmos. Oceans* **5**, 1–41 (1980).
Killworth, P. D., "On the motion of isolated lenses on a beta-plane," *J. Phys. Oceanogr.* **13**, 368–376 (1983).
Killworth, P. D., "On the propagation of isolated multilayer and continuously stratified eddies," *J. Phys. Oceanogr.* **16**, 709–716 (1986).
Longuet-Higgins, M. L., "The response of a stratified ocean to stationary or moving wind system," *Deep-Sea Res.* **12**, 923–973 (1965).
Matsuura, T. and Yamagata, T., "On the evolution of nonlinear planetary eddies larger than the radius of deformation," *J. Phys. Oceanogr.* **12**, 440–456 (1982).
Maximenko, N. and Yamagata, T., "Submesoscale Anomalies in the North Pacific Subarctic Front," *J. Geophys. Res.* **100**, 18459–18469 (1995).
Maximenko, N. A., Yamagata, T. and Okuda, K., "Frontal Convection in the Kuroshio and at the Subarctic Front," *Oceanology* **37**, 295–300 (1997).
McWilliams, J. C., "Submesoscale, coherent vortices in the ocean," *Rev. Geophys.* **23**, 165–182 (1985).
Nof, D., "On the β-induced movement of isolated baroclinic eddies," *J. Phys. Oceanogr.* **11**, 1662–1672 (1981).
Nof, D., "The translation of isolated cold eddies on a sloping bottom," *Deep-Sea Res.* **30**, 171–182 (1983).
Nof, D., "Joint vortices, eastward propagating eddies and migratory Taylor columns," *J. Phys. Oceanogr.* **15**, 1114–1137 (1985).
Nof, D. and Pichevin, T., "The retroflection paradox," *J. Phys. Oceanogr.* **26**, 2344–2358 (1996).
Pakyari, A. and Nycander, J., "Steady two-layer vortices on the beta-plane," *Dyn. Atmos. Oceans* **25**, 67–86 (1996).
Pichevin, T. and Nof, D., "The momentum imbalance paradox," *Tellus* **49A**, 298–319 (1997).
Richardson, P. L., Walsh, D., Armi, L., Schroder, M. and Price, J. F., "Tracking three Meddies with SOFAR floats," *J. Phys. Oceanogr.* **19**, 371–383 (1989).
Shapiro, G. I. and Meschanov, S. L., "Distribution and spreading of Red Sea Water and salt lens formation in the northwest Indian Ocean," *Deep-Sea Res.* **38**, 21–34 (1991).
Stern, M. E., "Minimal properties of planetary eddies," *J. Mar. Res.* **33**, 1–13 (1975).
Stommel, H. and Schott, F., "The beta spiral and the determination of the absolute velocity field from hydrographic station data," *Deep-Sea Res.* **24**, 325–329 (1977).
Sudo, H., "An analysis on the deep current of the ocean with its application to the circulation of the North Atlantic Ocean," *Japanese. J. of Geophysics* **4**, 1–70 (1965).
Talley, L. D., "Potential vorticity distribution in the North Pacific," *J. Phys. Oceanogr.* **18**, 89–106 (1988).
Talley, L. D., "An Okhotsk Sea water anomaly: implication for ventilation in the North Pacific," *Deep-Sea Res.* **38**, S171–190 (1991).
Talley, L. D., Nagata, Y., Fujimura, M., Iwao, T., Kono, T., Inagake, D., Hirai, M. and Okuda, K., "North Pacific Intermediate Water in the Kuroshio/Oyashio Mixed Water Region," *J. Phys. Oceanogr.* **25**, 475–501 (1995).

Tsunogai, S., Ono, T. and Watanabe, S., "Increase on total carbonate in the western North Pacific water and a hypothesis on missing sink of anthropogenic carbon," *J. Oceanogr.* **49**, 305–315 (1993).

Watanabe, Y. W., Harada, K. and Ishikawa, K., "Chlorofluorocarbons in the central North Pacific and southward spreading time of North Pacific Intermediate Water," *J. Geophys. Res.* **99**, 25195–25213 (1994).

Watanabe, Y. W., Ishida, A., Tamaki, M., Okuda, K. and Fukusawa, M., "Water column inventories of chlorofluorocarbons and production rate of intermediate water in the North Pacific," *Deep-Sea Res.* **44**, 1091–1104 (1997).

Whitehead, J. A., Stern, M. E., Flierl, G. R. and Klinger, B., "Experimental observations of baroclinic eddies on a sloping bottom," *J. Geophys. Res.* **95**, 9585–9610 (1990).

Yamagata, T., "On nonlinear planetary waves: A class of solutions missed by the quasi-geostrophic approximation," *J. Oceanogr. Soc. Jpn.* **38**, 236–244 (1982).

Yamagata, T., Sakamoto, K. and Arai, M., "Locally-induced nonlinear modes and multiple equilibria in planetary fluids," *PAGEOPH* **133**, 733–748 (1990).

Yasuda, I., Okuda, K. and Shimizu, Y., "Distribution and modification of North Pacific Intermediate Water in the Kuroshio-Oyashio interfrontal zone," *J. Phys. Oceanogr.* **26**, 448–465 (1996).

Zatsepin, A. G. and Didkovskii, V. L., "On one mechanism of vortical structure formation in the oceanic slope zone," *Doklady Akademii Nauk* **347**, 109–112 (1996).